STRUCTURAL SCIENCE
CRYSTAL ENGINEERING
MATERIALS

Volume 73 (2017)

Supporting information for article:

The structure directing amine changes everything: Structures and optical properties of two-dimensional thiostannates

Mette Ø. Filsø, Iman Chaaban, Amer Al Shehabi, Jørgen Skibsted and Nina Lock

The structure directing amine changes everything: Structures and optical properties of two-dimensional thiostannates

Mette Ø. Filsø,[a] Iman Chaaban,[b] Amer Al Shehabi,[b] Jørgen Skibsted[c] and Nina Lock[d]*

[a]Center for Materials Crystallography, Department of Chemistry and iNANO, Aarhus University, Langelandsgade 140, DK-8000 Aarhus C, Denmark

[b]iNANO, Aarhus University, Gustav Wieds Vej 14, DK-8000 Aarhus C, Denmark

[c]Department of Chemistry and iNANO, Aarhus University, Langelandsgade 140, DK-8000 Aarhus C, Denmark

[d]iNANO and Department of Chemistry, Aarhus University, Gustav Wieds Vej 14, DK-8000 Aarhus C, Denmark

Corresponding author: nlock@chem.au.dk

Powder X-ray diffraction

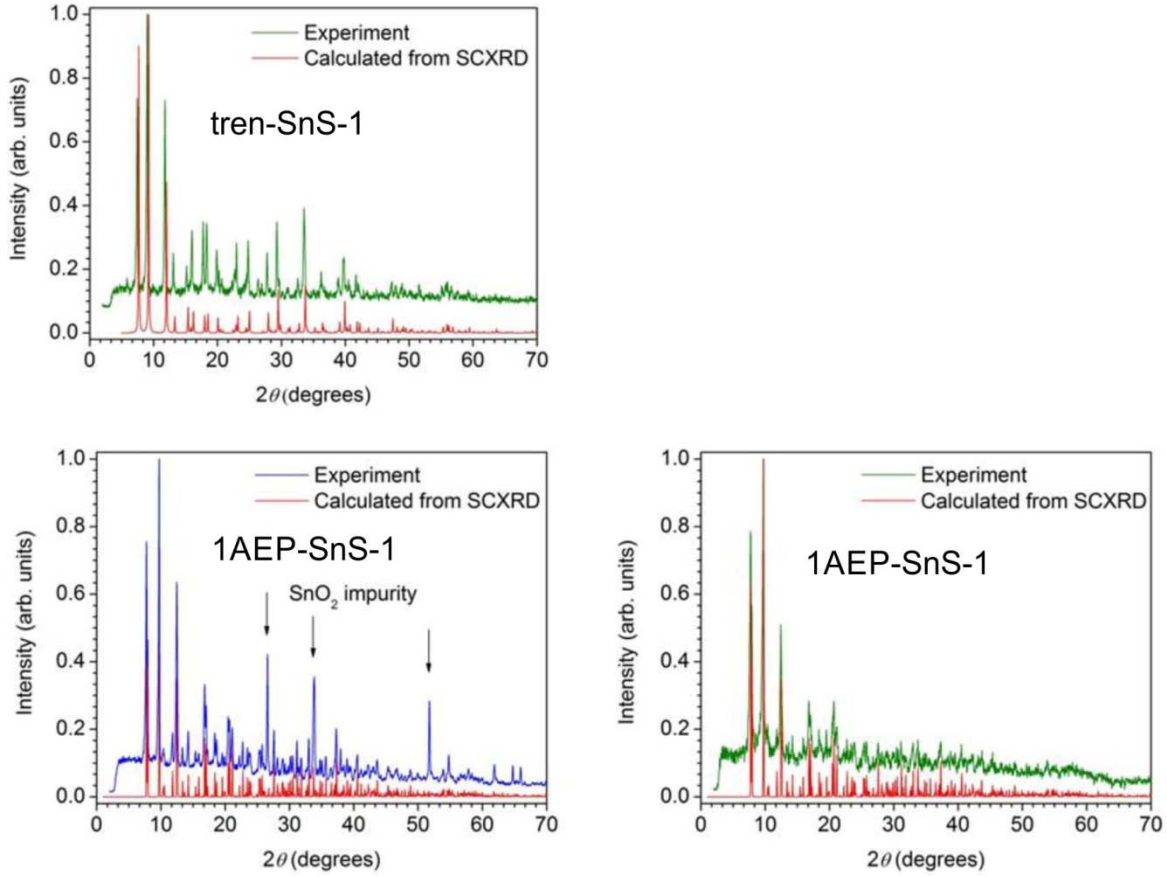

Fig. S1.

Room temperature powder diffraction data (blue/green) for tren-SnS-1 (top) and 1AEP-SnS-1 (bottom) compared with a theoretical powder pattern based on structural data from single crystal diffraction (red). Data has been normalized to the most intense reflection. By using a stoichiometric SnO_2:S mixture of 3:7 or a 1:6 ratio, SnO_2 impurities were observed for the synthesis of 1AEP-SnS-1. No crystalline impurities are observed by using an SnO_2:S ratio of 1:10. tren-SnS-1 data are based on a stoichiometric SnO_2:S mixture and only a small SnO_2 impurity is observed.

Diffuse reflectance spectroscopy

The measured diffuse reflectance spectroscopy data were transformed to the Kubelka-Munk function F_{KM}, where R is the measured reflectance data:

$$F_{\mathrm{KM}} = \frac{(1-R)^2}{2R}$$

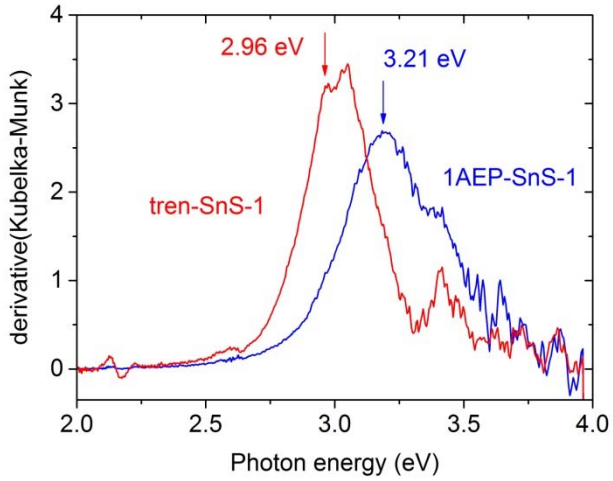

Fig. S2.

The first derivative of F_{KM} for tren-SnS-1 and 1AEP-SnS-1. The band gap was determined as the first maximum of the numerical first derivative of F_{KM}, which is one of the methods for band gap determination reviewed by Nowak *et al.* (2009).

SEM

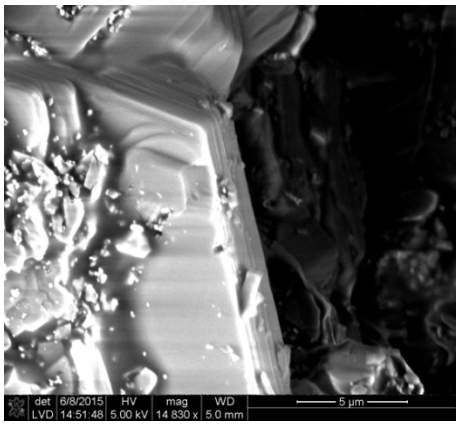

Fig. S3.

SEM image of tren-SnS-1 indicating presence of crystals with hexagonal shape.

Intramolecular ring formation

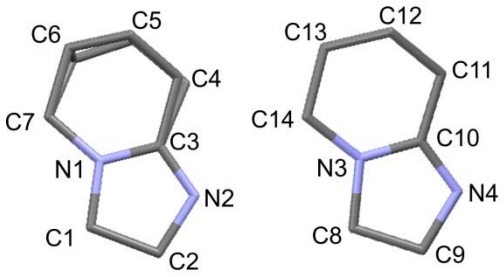

cation 1 cation 2

Cation 1	*d* (Å)	Cation 2	*d* (Å)
N1-C3	1.304(12)	N3-C10	1.308(13)
C3-N2	1.293(13)	C10-N4	1.302(13)
N2-C2	1.481(14)	N4-C9	1.455(13)
C2-C1	1.523(14)	C9-C8	1.518(13)
C1-N1	1.459(12)	C8-N3	1.450(12)
C3-C4A/C3-C4B	1.484(16)/1.472(28)	C10-C11	1.491(14)
C4A-C5A/C4B-C5B	1.536(19)/1.527(31)	C11-C12	1.498(13)
C5A-C6A/C5B-C6B	1.512(28)/1.503(38)	C12-C13	1.529(15)
C6A-C7/C6B-C7	1.476(16)/1.480(27)	C13-C14	1.492(14)
C7-N1	1.452(12)	C14-N3	1.457(12)
Abs(Tors(N1-C3-N2-C2))	2.44	Abs(Tors(N3-C10-N4-C9))	4.93

Table S1.

Structural information on the cations in 1AEP-SnS-1 based on 100 K single crystal diffraction data (where the dynamic disorder is lower than at 300 K). The carbon atoms C4, C5, and C6 of cation 1 are disordered over two positions. In 1AEP-SnS-1 the scattering contribution of the cations is relatively small in comparison with the electron rich SnS anionic sheets. This may explain the relatively large uncertainties.

NMR

Solid state ^{119}Sn NMR data were measured on 1AEP-SnS-1. The peaks were assigned by measuring two spectra at different spinning rates (ν_R), which influence the distance between the spinning sidebands. The peaks that do not shift with changing spinning rate were recognized as the isotropic peaks. The asymmetric unit of 1AEP-SnS-1 contains three crystallographically different tin atoms. Two of the Sn-atoms appear to have the same chemical shift (most likely Sn2 and Sn3). NMR data are presented in Fig. S4 and Table S2.

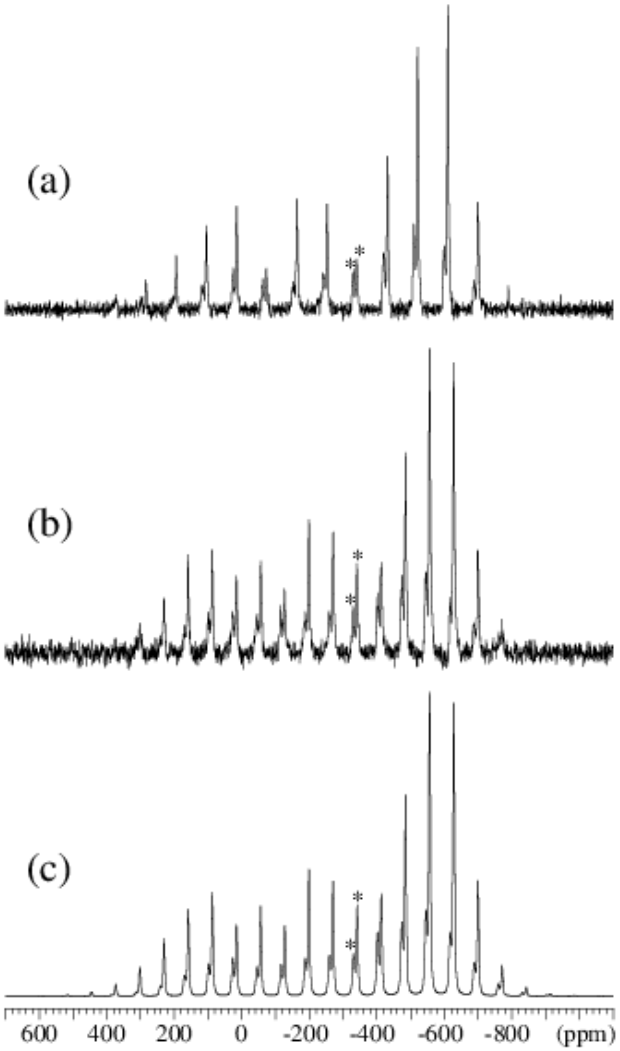

Fig. S4.

^{119}Sn MAS NMR spectra (7.05 T) of 1AEP-SnS-1 acquired with spinning speeds of (a) ν_R = 10.0 kHz and (b) ν_R = 8.0 kHz, using ^{1}H decoupling (TPPM, $\gamma B_2/2\pi$ = 62 kHz). (c) Optimized simulation of the spectrum in (b), employing manifolds of spinning sidebands for two distinct Sn sites and corresponding to the optimized ^{119}Sn chemical shift anisotropy parameters listed in Table S2. The isotropic peaks are indicated by asterisks.

Sn site	δ_{iso} (ppm)	δ_σ (ppm)	η_σ
Sn	-331 ± 2	-578 ± 15	0.44 ± 0.06
Sn2, Sn3	-342 ± 1	-667 ± 10	0.12 ± 0.04

Table S2.

^{119}Sn isotropic chemical shifts (δ_{iso}) and chemical shift anisotropy parameters (δ_σ and η_σ) for 1AEP-SnS-1. Data determined from ^{119}Sn MAS NMR spectra acquired at 7.05 T. The isotropic chemical shifts are relative to $(CH_3)_4Sn$. The shift anisotropy parameters are defined as: $\delta_\sigma = \delta_{iso} - \delta_{zz}$ and $\eta_\sigma = (\delta_{xx} - \delta_{yy})/\delta_\sigma$, using the convention: $|\delta_{zz} - \delta_{iso}| \geq |\delta_{xx} - \delta_{iso}| \geq |\delta_{yy} - \delta_{iso}|$.

Tin atom coordination environment

Bridges					
tren-SnS-1 bridge		1AEP-SnS-1 *symmetric* bridge		1AEP-SnS-1 *asymmetric* bridge	
distance (Å)		distance (Å)		distance (Å)	
Sn1a-S3	2.401(3)	Sn1a-S5	2.428(2)	Sn2-S7	2.397(2)
Sn1a-S3’	2.535(3)	Sn1a-S6	2.473(2)	Sn2-S8	2.566(2)
Sn1b-S3	2.535(3)	Sn1b-S5	2.428(2)	Sn3-S7	2.556(2)
Sn1b-S3’	2.401(3)	Sn1b-S6	2.473(2)	Sn3-S8	2.402(2)
angle (°)		angle (°)		angle (°)	
Sn1a-S3-Sn1b	91.02(11)	Sn1a-S5-Sn1b	91.91(8)	Sn2a-S7-Sn3c	90.84(6)
Sn1a-S3’-Sn1b	91.02(11)	Sn1a-S6-Sn1b	89.78(8)	Sn2a-S8-Sn3c	90.51(6)
S3-Sn1a-S3’	88.98(11)	S5-Sn1a-S6	89.15(6)	S7-Sn2a-S8	88.41(5)
S3-Sn1b-S3’	88.98(11)	S5-Sn1b-S6	89.15(6)	S7-Sn3c-S8	88.54(5)
torsion angle (°)		torsion angle (°)		torsion angle (°) (Abs. value)	
Sn1a-S3-Sn1b-S3’	0.00	Sn1a-S5-Sn1b-S6	0.00	Sn2a-S8-Sn3c-S7	9.54

Table S3.

The table contains information on the three bridges in 1AEP-SnS-1 and tren-SnS-1. The sign of the torsion angle for the asymmetric bridge depends on the chirality of the crystal. Therefore, the absolute value is shown.

Selected published R-SnS-1 layered structures

Selected R-SnS-1 layered structures (reported in the Cambridge Structural Database)			
Compound	Torsion angle (abs)	Layer top-view	Layer side-view
GIRHEU $(C_8H_{20}N^+)_{1.5n}(NH_4^+)_{0.5n}(Sn_3S_7^{2-})_n$ (Jiang *et al.*, 1998) $P3_121$ (no. 152) hexagonal Et_4N^+, NH_4^+	1.29° (Sn1-S3-Sn2-S6) 1.62° (Sn3-S7-Sn3'-S7')	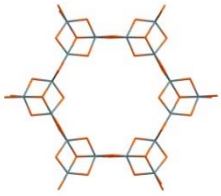	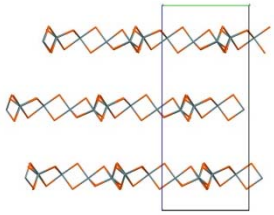
GIRHIY $(C_8H_{20}N^+)_{2n}(Sn_3S_7^{2-})_n$ (Jiang *et al.*, 1998) $P2_1/n$ (no. 14) Monoclinic Et_4N^+	0.00° (Sn1-S7-Sn1'-S7') 5.68° (Sn2-S5-Sn3-S6)	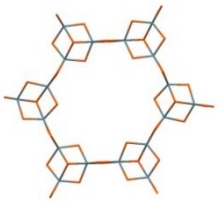	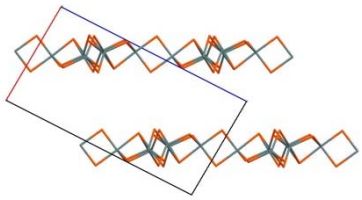
PESQAF01 $(C_6H_{13}N_2^+)_{2n}(Sn_3S_7^{2-})_n(H_2O)_n$ (Jiang *et al.*, 1998) C2/c (no. 15) Monoclinic $DABCOH^+$	2.04° (Sn2-S7-Sn2'-S7') 7.09° (Sn1-S5-Sn3-S6)	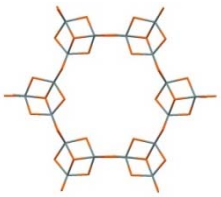	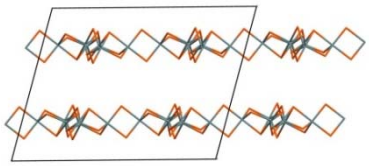
WINJEI $(C_3H_{10}N^+)_{2.04n}(Sn_{18}S_{42}^{12-})_{0.17n}.(H_2O)_{0.72n}$ (Tan *et al.*, 1995) C2/c (no. 15) monoclinic Me_3NH^+, decomposition product	4.08° (Sn1-S5-Sn2-S6) 3.14° (Sn3-S3-Sn3'-S3')		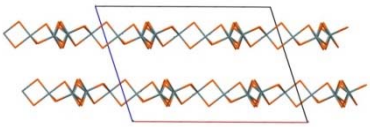
YAZNOC $(C_4H_{12}N^+)_{2n}(Sn_3S_7^{2-})_n(H_2O)_n$ (Parise *et al.*, 1994) $P2_1/n$ (no. 14) Monoclinic Me_4N^+	9.53° (Sn1-S3-Sn3-S4) 0.00° (Sn2-S5-Sn2'-S5')	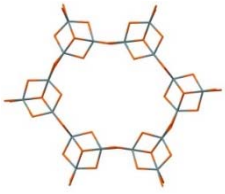	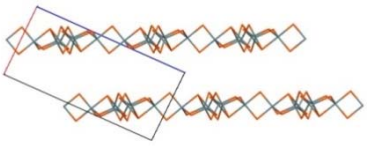

YOHJOU01 $(C_4H_{12}N^+)_{4n}(Sn_6S_{14}^{4-})_n$ (Marsh, 2004; Jiang *et al.*, 1994) C2/c (no. 15) Monoclinic Et_4N^+	3.35° (Sn1-S6-Sn1'-S6) 3.59° (Sn2-S5-Sn3-S7)		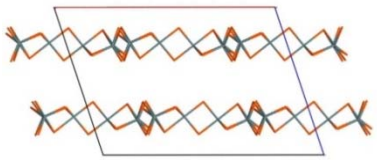

Table S4.

The structure name and chemical formulae according to the CSD database, the crystal symmetry, the structure directing agent and the bridge torsion angles are shown along with plots of the structures. There are three tin atoms in the asymmetric unit of all structures in the table. The refined cations between the layers are not shown for clarity.

Hirshfeld surface calculations

The Hirshfeld surface method is based on the concept by Hirshfeld dividing electron density of a molecule into atomic fragments. A generalization of this concept enabled to extract molecular fragments from a crystal by defining the molecular weight function $w(\mathbf{r})=\rho_{\text{promolecule}}(\mathbf{r})/\rho_{\text{procrystal}}(\mathbf{r})$. The promolecule density is the sum of spherically averaged atomic electron density functions centered at the atomic positions for the molecular fragment in focus, and the procrystal density is the analogously defined density of the surrounding crystal. Spackman *et al.* suggested to partition space into regions where the promolecule density dominates, *e.g.* at $w(\mathbf{r})=0.5$, and thereby defined the Hirshfeld surface. The concept is not only applicable to molecular fragments but also to atoms in the crystal, the latter is called atomic Hirshfeld surface (AHS). This tool allows for analysis of bonding pattern in non-molecular crystal structures as well as analyzing the atomic environment (McKinnon *et al.*, 2004).

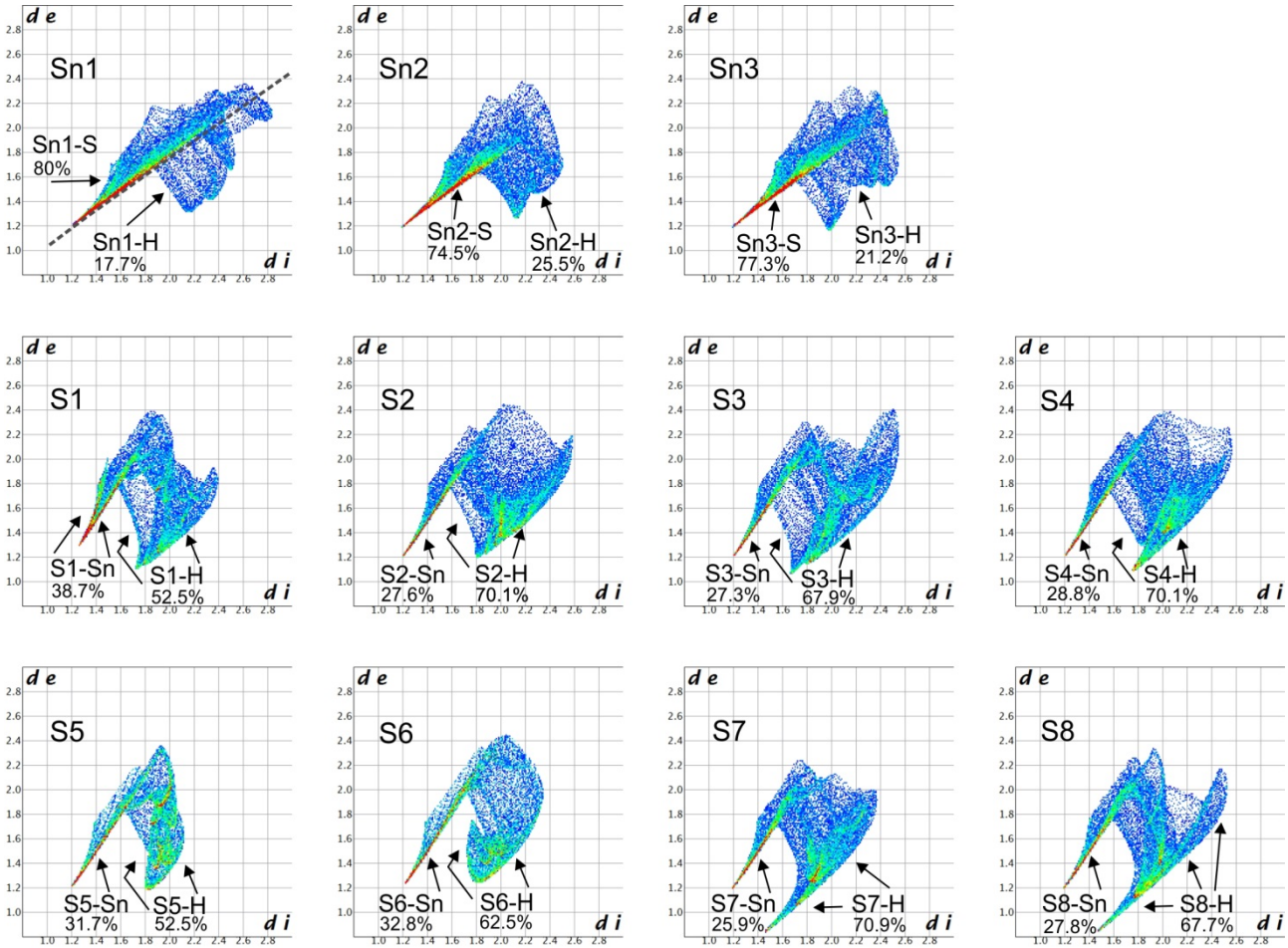

Fig. S5.

Finger print plot of all atoms in 1AEP-SnS-1 based on 100 K single crystal diffraction data. Besides the covalent bond interactions (observed in the region above the dotted line shown in the top left plot) the dominating interactions are Sn-H/S-H interactions. The strongest contributions to the surface area of the AHS are shown.

References

Jiang, T., Lough, A., Ozin, G. A., Bedard, R. & Broach, R. (1998). *J. Mater. Chem.* **8,** 721-732.

Jiang, T., Ozin, G. A. & Bedard, R. L. (1994). *Adv. Mater.* **6,** 860-865.

Marsh, R. E. (2004). *Acta Cryst.* **B60,** 252-253.

McKinnon, J. J., Spackman, M. A. & Mitchell, A. S. (2004). *Acta Cryst.* **B60,** 627-668.

Nowak, M., Kauch, B. & Szperlich, P. (2009). *Rev. Sci. Instrum.* **80,** 046107-3.

Parise, J. B., Ko, Y., Rijssenbeek, J., Nellis, D. M., Tan, K. & Koch, S. (1994). *J. Chem. Soc. , Chem. Commun.* 527.

Tan, K., Ko, Y. & Parise, J. B. (1995). *Acta Cryst.* **C51,** 398-401.